

Preclinical development of ozuriftamab vedotin (BA3021), a novel ROR2-specific conditionally active biologic antibody–drug conjugate

Hwai Wen Chang, Gerhard Frey, Jing Wang, Haizhen Liu, Charles Xing, Jian Chen, William J. Boyle & Jay M. Short

To cite this article: Hwai Wen Chang, Gerhard Frey, Jing Wang, Haizhen Liu, Charles Xing, Jian Chen, William J. Boyle & Jay M. Short (2025) Preclinical development of ozuriftamab vedotin (BA3021), a novel ROR2-specific conditionally active biologic antibody–drug conjugate, mAbs, 17:1, 2490078, DOI: [10.1080/19420862.2025.2490078](https://doi.org/10.1080/19420862.2025.2490078)

To link to this article: <https://doi.org/10.1080/19420862.2025.2490078>



© 2025 BioAtla inc. Published with license by Taylor & Francis Group, LLC.



[View supplementary material](#)



Published online: 09 Apr 2025.



[Submit your article to this journal](#)



[View related articles](#)




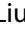

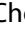




[View Crossmark data](#)

REPORT



Preclinical development of ozuriftamab vedotin (BA3021), a novel ROR2-specific conditionally active biologic antibody–drug conjugate

Hwai Wen Chang , Gerhard Frey , Jing Wang , Haizhen Liu , Charles Xing , Jian Chen , William J. Boyle , and Jay M. Short 

Research & Development, BioAtla Inc, San Diego, CA, USA

ABSTRACT

Receptor tyrosine kinase-like orphan receptor (ROR2) has been identified as a highly relevant tumor-associated antigen in a variety of cancer indications of high unmet medical need, including melanoma, renal cell carcinoma, osteosarcoma, gastrointestinal stromal tumor, colorectal cancer, pancreatic ductal adenocarcinoma, and non-small cell lung cancer. Overexpression of ROR2 often correlates with advanced disease or poor prognosis, making it an attractive target for cancer therapy. We developed a novel, conditionally active biologic (CAB) antibody–drug conjugate (ADC), ozuriftamab vedotin (BA3021), which binds to ROR2 only in the acidic tumor microenvironment. In healthy tissue, binding to ROR2 is greatly reduced by a novel selection mechanism using physiological chemicals as protein-associated chemical switches (PaCS). The CAB anti-ROR2 ADC displays the anticipated binding properties and mediates potent lysis of ROR2-positive cancer cell lines. *In vivo*, BA3021 has potent and durable antitumor activity in human cancer xenograft mouse models, including patient-derived xenograft models. In non-human primates, BA3021 was well tolerated at doses of up to 10 mg/kg and showed excellent stability *in vivo*. These preclinical results indicate that CAB anti-ROR2 ADC is efficacious and well tolerated and may be a promising treatment for cancer patients with ROR2-expressing tumors.

ARTICLE HISTORY

Received 20 December 2024
Revised 1 April 2025
Accepted 2 April 2025

KEYWORDS

ADC; conditionally active;
ROR2; tumor targeting

Introduction

Receptor tyrosine kinase orphan receptor 2 (ROR2) is a member of the ROR family of type I transmembrane receptors with ligand-binding extracellular regions and intracellular tyrosine kinase domains.^{1,2} ROR2 interacts with Wnt3a and Wnt5a, which activate canonical and non-canonical Wnt signaling pathways. Wnt signaling is essential for embryonic development, including cell polarization, motility, migration, and invasion, processes in which ROR2 has also been implicated.^{3–7} Mice deficient in ROR2 are viable for a short time after birth, but have heart, nervous system, and skeletal defects.^{8–10} Homozygous mutations in ROR2 are associated with the human skeletal diseases, including Robinow syndrome and brachydactyly type B.^{11,12} Additionally, ROR2 was found to be meaningfully overexpressed in human papilloma virus (HPV) – associated squamous cell oropharyngeal cancer.¹³ Further studies have shown that the HPV oncogenic E6 and/or E7 proteins drive increased ROR2 expression.¹⁴ Finally, expression of ROR2 decreases during fetal development,¹⁵ but a recent report indicates that ROR2 is expressed in a variety of healthy tissues in adults (colon, esophagus, and reproductive tissues).¹⁶

ROR2 was first cloned from the neuroblastoma cell line, SH-SY5Y,^{17,18} and subsequently shown to be highly expressed in osteosarcoma,¹⁹ renal cell carcinoma,^{20–22} melanoma,²³ colorectal cancer,²⁴ pancreatic ductal adenocarcinoma,²⁵ non-small cell lung carcinoma (NSCLC),²⁶ squamous cell

carcinoma of the head and neck,²⁷ gastrointestinal stromal tumor (GIST),²⁸ and breast cancer.^{29,30} In many of these cancer types, expression of ROR2 correlates with advanced stage of disease and/or poor prognosis.^{31–33} Due to its association with increased aggression in many types of cancer and its location on the cell surface, ROR2 has been identified as a potential target for cancer therapeutic development.³⁴

Antibody–drug conjugates (ADCs) represent a rapidly expanding class of antitumor therapeutics that utilize monoclonal antibodies (mAbs) to deliver potent cytotoxic agents directly to tumor cells by targeting specific tumor-associated antigens.³⁵ Factors such as the distribution of target antigens in normal tissue, the efficiency of ADC internalization by target cells, the stability of the linker-payload in circulation, and the clearance of free cytotoxic agents significantly influence the therapeutic efficacy and safety profile of each ADC.

Acidic extracellular pH is a key characteristic of the tumor microenvironment (TME) because of the glycolytic metabolism of cancer cells that underpins the continuous replication of cancer cells.³⁶ Conditionally active biologic (CAB) technology is an innovative platform for generating antibodies that exploits the differential binding of naturally occurring Protein-associated Chemical SwitchesTM (PaCSTM) on target molecules.³⁷ This approach results in antibodies that exhibit minimal/no binding to target antigens in healthy tissue (under normal physiological conditions with pH ≥ 7.4), while demonstrating robust binding affinity in the acidic TME (pH 5.3 to 6.7).^{37,38} The measured

CONTACT Hwai Wen Chang  cchang@bioatla.com 

 Supplemental data for this article can be accessed online at <https://doi.org/10.1080/19420862.2025.2490078>

© 2025 BioAtla inc. Published with license by Taylor & Francis Group, LLC.

This is an Open Access article distributed under the terms of the Creative Commons Attribution-NonCommercial License (<http://creativecommons.org/licenses/by-nc/4.0/>), which permits unrestricted non-commercial use, distribution, and reproduction in any medium, provided the original work is properly cited. The terms on which this article has been published allow the posting of the Accepted Manuscript in a repository by the author(s) or with their consent.

extracellular pH in tumors depends greatly on the method used. For example, experiments with pH electrodes or magnetic resonance imaging have shown a pH range from pH6.3 to pH7.3 for a wide variety of cancer types and animal models. However, these methods lack spatial resolution at the single cell level. Using pH-sensitive nanopores, it has been shown that the pH at the cell surface is below pH6.0 based on the high local concentration of secreted lactic acid.³⁹ In tumors, low pH measurements indicate that all of the tumor cells have an acidic extracellular surface (\leq pH 6.5), including cells located in aerobic regions and close to the interphase with normal cells.⁴⁰ Leveraging CAB technology, we developed BA3021, a novel anti-ROR2 CAB-ADC designed to target tumor tissues and potentially enhance the therapeutic index by reducing on-target, off-tumor toxicity. Here, we present the results of several pharmacological studies conducted *in vitro* and *in vivo*. These studies collectively demonstrated that BA3021 selectively binds to human and cynomolgus monkey ROR2 under acidic conditions typical of the TME, while exhibiting reduced binding under normal alkaline physiological conditions. BA3021 induced the cytotoxicity of human tumor cell lines expressing ROR2 *in vitro* and inhibited tumor growth in human tumor xenografts *in vivo*. Moreover, BA3021 demonstrated favorable tolerability in non-human primate (NHP) toxicity studies. These findings underscore the potential of BA3021 as a promising strategy for cancers expressing ROR2. Early clinical results with BA3021 (ozuriftamab vedotin) have shown promising outcomes in patients with advanced malignancies, including melanoma and head and neck squamous cell carcinoma.⁴¹

Materials and methods

Generation of ROR2-specific conditionally active antibodies and drug conjugates

Antibodies against human ROR2 were developed by immunizing BALB/c mice (Green Mountain Antibodies) with a peptide (VLDPNPLGPLDGQDGC, New England Peptides) specific for ROR2 conjugated to keyhole limpet hemocyanin (KLH) for immunization and to bovine serum albumin (BSA) for counter screening. Hybridoma clones producing ROR2-specific mAbs were identified by enzyme linked immunosorbent assay (ELISA) with ROR2 peptides and by cell-based ELISA using Chinese hamster ovary (CHO) cells expressing human ROR2 on the cell surface.

Variable domains from hybridomas were cloned, expressed as human IgG1/kappa chimeras, and further characterized for their binding and *in vitro* functional activities. Selected clones were conjugated with monomethyl auristatin E (MMAE) and tested for cell-killing activity *in vitro*. Chimeric clone BA-048-2-11 was humanized using BioAtla's proprietary Express HumanizationTM protocol. One of the humanized variants, clone BA-048-hum2-11, was selected for further engineering and the development of a CAB antibody³⁷ that binds to human ROR2-ECD at pH6.0 (TME conditions) and has reduced binding at pH7.4 (normal alkaline physiological conditions) (Figure S1).

Lead ROR2 CAB clone BA302 and isotype control clone B12 (specific for GP120) were conjugated with mc-vc-PAB-

MMAE containing a valine-citrulline protease cleavable dipeptide as described.⁴² BA3021, the resulting ADC from clone BA302 (drug-to-antibody ratio 4:1, DAR4) (Figure 1a) was characterized *in vitro* and *in vivo* and is described further in this report.

Cell lines and cell culture

LCLC-103 h, a human large cell lung carcinoma cell line (DSMZ, catalog no. ACC384), was cultured in RPMI1640 media (Gibco, catalog no. 11875-085) supplemented with 10% fetal bovine serum (FBS) (Gibco, catalog no. 16140-071). SK-MEL-5, a human melanoma cell line (ATCC, catalog no. HTB-70), and HT-1080, a human fibrosarcoma cell line (ATCC, catalog no. CCL-21), were cultured in MEM media (Gibco, catalog no. 11095-072) supplemented with 10% FBS.

293-F cells were derived from the 293 cell line, a primary embryonal human kidney cell line transformed with sheared human adenovirus type 5 DNA (ThermoFisher, catalog no. R79007). 293-F cells expressing human ROR2 extracellular domain (ECD) (293-HuROR2) or cynomolgus ROR2 ECD (293-CynoROR2) on the cell surface were created at BioAtla and cultured in MEM (Gibco, catalog no. 11095-072) supplemented with 10% FBS and 1 mg/mL of G418 (Invivogen, catalog no. ant-gn-5). All cells were maintained at 37°C and 5% CO₂ in a humidified atmosphere and routinely sub-cultured twice per week. Cells were harvested in an exponential growth phase and used for the experiments described here.

pH affinity ELISA using BA3021

Human recombinant ROR2 extracellular domain fused to mouse Fc (HuROR2-mFc, BioAtla) was immobilized in the wells of a 96-well ELISA plate at 1 μ g/mL in carbonate/bicarbonate coating buffer (Sigma, catalog no. C3041-100CAP) overnight at 4°C. Plates were blocked with either pH6.0 ELISA assay incubation buffer (PBS with 2.5 g/L sodium bicarbonate, 2% nonfat milk, pH6.0) or pH7.4 ELISA assay incubation buffer (PBS with 2.5 g/L sodium bicarbonate, 2% nonfat milk, pH7.4) at room temperature for 1 h, then washed with the corresponding pH ELISA wash solution (PBS with 2.5 g/L sodium bicarbonate, 0.05% Tween-20). BA3021 ADC was serially diluted in the corresponding pH ELISA assay incubation buffer and added to the previously blocked and washed wells. ELISA plates containing diluted antibodies were sealed and incubated at room temperature for 1 h with shaking. The plates were washed three times with the corresponding pH ELISA wash buffer, then 100 μ L of anti-human IgG horseradish peroxidase (HRP) conjugate (Promega, catalog no. W4031) diluted 1:2,500 in the corresponding pH ELISA assay incubation buffer was added to each well. Subsequently, the plates were sealed and incubated at room temperature for 1 h with shaking. Following incubation, the plates were washed three times with the corresponding pH ELISA wash buffer. About 100 μ L of 3,3', 5,5' tetramethylbenzidine dihydrochloride (TMB) peroxidase substrate solution (ThermoFisher, catalog no. 002023) was added to each well, and the reactions were stopped after 3 min with 100 μ L of 0.1

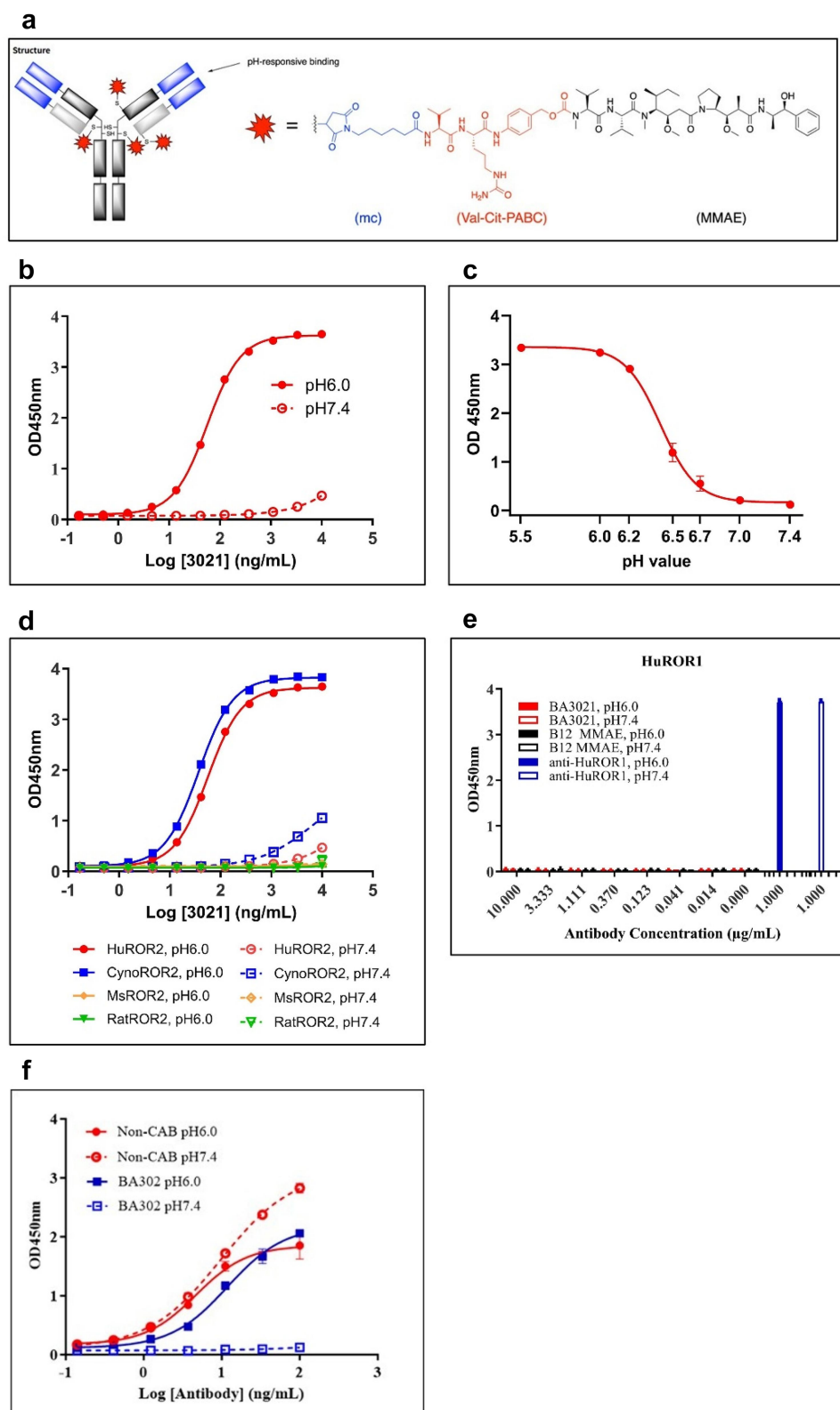


Figure 1. *In vitro* characterization of BA3021. **a:** Structure Overview. BA3021 consists of an IgG1 antibody (BA302) with pH-responsive binding to ROR2. In average, 4 mMAE toxins are conjugated to each antibody molecule via maleimide and a protease cleavable vedotin linker. **b:** pH affinity ELISA. Binding of BA3021 to human ROR2 was determined by ELISA with a series of antibody concentrations as indicated on the graph. BA3021 was captured with huROR2 immobilized on the plate. Bound ADC was detected with anti-human IgG-HRP conjugate. The EC₅₀ values of BA3021 at pH6.0 (red filled circles) or pH7.4 (red open circles) were determined by GraphPad Prism software. x-axis: log ADC concentration in ng/mL; y-axis: Optical Density at 450 nm (OD_{450nm}). **c:** pH range ELISA. Binding of BA3021 to human ROR2 at different pH values was determined by ELISA. HuROR2 was immobilized on a plate and incubated with BA3021 at pH 5.5, 6.0, 6.2, 6.5, 6.7, 7.0, or 7.4. After washing at the same pH, bound BA3021 was detected with an anti-human IgG-HRP conjugate. The pH inflection point (50% binding activity compared to pH6.0) was at pH6.4. x-axis: pH values; y-axis: Optical Density at 450 nm (OD_{450nm}). **d:** Cross Species ELISA. Binding of BA3021 to human (HuROR2, red circles), cynomolgus (CynoROR2, blue squares), mouse (MsROR2, orange diamonds), and rat (RatROR2, green triangles) ROR2 at pH6.0 (full symbols) and pH7.4 (open symbols) was determined by ELISA. ROR2 proteins were immobilized in the wells and incubated with BA3021 at pH6.0 or pH7.4. After washing at the same pH, bound BA3021 was detected with an anti-human IgG-HRP conjugate. BA3021 shows a strong and very similar binding to human and cynomolgus ROR2 at pH6.0, but only weak binding at pH7.4. No binding was

N HCl (Beijing Reagent, catalog no. G81788B). The OD at 450 nm was collected using a Microplate Spectrophotometer (Molecular Device, SpectraMax 190). Half-maximal effective concentration (EC₅₀) values for binding to human ROR2 ECD at pH6.0 and pH7.4 were determined using the nonlinear fit model (variable slope, four parameters) of GraphPad Prism version 7.03.

Binding to ROR1 antigen was tested following the ELISA protocol with ROR2.

pH affinity ELISA using non-CAB and BA302 naked antibody

Human recombinant ROR2 extracellular domain fused to mouse Fc (HuROR2-mFc, BioAtla) was immobilized in the wells of a 96-well ELISA plate at 1 µg/mL in carbonate/bicarbonate coating buffer (Sigma, catalog no. C3041-100CAP) overnight at 4°C. Plates were blocked with either pH6.0 ELISA assay incubation buffer (Krebs-Ringer bicarbonate buffer from Sigma, catalog no. K4002 with 1.26 g/L sodium bicarbonate, 0.09 g/L L-lactic acid, 1% BSA, pH6.0) or pH7.4 ELISA assay incubation buffer (Krebs-Ringer bicarbonate buffer from Sigma, catalog no. K4002 with 1.26 g/L sodium bicarbonate, 0.09 g/L L-lactic acid, 1% BSA, pH7.4) at room temperature for 1 h, then washed with the corresponding pH ELISA assay incubation buffer. Non-CAB and BA302 naked antibodies were serially diluted in the corresponding pH ELISA assay incubation buffer and added to the previously blocked and washed wells. ELISA plates containing diluted antibodies were sealed and incubated at room temperature for 1 h with shaking. The plates were washed three times with the corresponding pH ELISA assay buffer, and then 100 µL of anti-human IgG horseradish peroxidase (HRP) conjugate (Promega, catalog no. W4031) diluted 1:2,500 in the corresponding pH ELISA assay incubation buffer was added to each well. Subsequently, the plates were sealed and incubated at room temperature for 1 h with shaking. Following incubation, the plates were washed 3 times with the corresponding pH ELISA wash buffer. About 100 µL of TMB Peroxidase substrate solution (ThermoFisher, catalog no. 002023) was added to each well, and the reactions were stopped after 3 min with 100 µL of 0.1 N HCl (Beijing Reagent, catalog no. G81788B). The OD at 450 nm was collected using a Microplate Spectrophotometer (Molecular Device, SpectraMax 190). Half-maximal effective concentration (EC₅₀) values for binding to human ROR2 ECD at pH6.0 and pH7.4 were determined using the nonlinear fit model (variable slope, four parameters) of GraphPad Prism version 7.03.

pH range ELISA

The binding activity of BA3021 to ROR2 was tested in a range of pH ELISA assay conditions (pH5.5, 6.0, 6.2, 6.5, 6.7, 7.0, and 7.4) as described above (pH affinity ELISA). The BA3021 pH inflection point that demonstrated 50% binding activity compared to pH6.0 (set as 100%) was determined using the nonlinear fit model (variable slope, 4 parameters) of GraphPad Prism version 7.03.

Cross-species ELISA

Human recombinant ROR2 antigen (BioAtla), cynomolgus recombinant ROR2 antigen (BioAtla), mouse recombinant ROR2 antigen (BioAtla), and rat recombinant ROR2 antigen (BioAtla) were immobilized in the wells of 96-well ELSA plates at 1 µg/mL in carbonate bicarbonate coating buffer (Sigma, catalog no. C3041-100CAP) overnight at 4°C. The cross-species ELISA was performed following the same method as described in pH affinity ELISA and the data were analyzed using the nonlinear fit model (variable slope, four parameters) of GraphPad Prism version 7.03.

Antibody–drug conjugate preparation

A solution of naked mAb BA302 (5 mg/mL in PBS with 100 mm arginine, 20 mm EDTA, pH6.7) was treated with 3 equivalents of tris(2-carboxyethyl)-phosphine (TCEP, Bond-Breaker catalog no. 77720) for 1 h at 25°C. Then, 10 molar equivalents of maleimidocaproyl valine-citrulline-p-aminobenzyloxycarbonyl-monomethyl auristatin E (mc-vc-PAB-MMAE, MedChemExpress, catalog no. 646502-53-6) were added to the fully reduced antibody, and the mixture was incubated for 1 h at 25°C. Excess reagents were removed by size-exclusion chromatography. The DAR was determined by hydrophobic interaction chromatography (Proteomix HIC Butyl-NP5 column).

pH flow cytometry

The binding affinity of BA3021 to human and cyno-ROR2-expressing 293 stable cells, as well as human ROR2-expressing tumor cell lines was measured by flow cytometry under pH6.0 and pH7.4 conditions. B12 (anti-GP120 antibody) conjugated to MMAE (B12-MMAE) at a similar DAR was used as the isotype control. Briefly, the cells in the log phase were detached and seeded in 96-well round bottom plates and then washed with a pH flow cytometry assay buffer (PBS with 2.5 g/L sodium bicarbonate and 1% BSA) at pH6.0 or pH7.4 and pelleted with centrifuge. The antibodies that were serially

detected with mouse or rat ROR2. x-axis: log ADC concentration in ng/mL; y-axis: Optical Density at 450 nm (OD450nm). e: Specificity ELISA. Binding of BA3021 and an isotype control ADC (B12 mmAE) to human ROR1 (HuROR1) was determined by ELISA. HuROR1 protein was immobilized in the wells and incubated with varying concentrations of BA3021 or B12 mmAE at pH6.0 or pH7.4. After washing at the same pH, bound ADC was detected with an anti-human IgG-HRP conjugate. No binding of BA3021 (or the isotype ADC) to human ROR1 was detected. The presence of human ROR1 in the wells was confirmed with an anti-ROR1 antibody. f: pH affinity ELISA. Binding of BA302 and non-CAB antibody to human ROR2 was determined by ELISA with a series of antibody concentrations as indicated on the graph. Antibody was captured with huROR2 immobilized on the plate. Bound 302 or non-CAB antibody was detected with anti-human IgG-HRP conjugate. The EC₅₀ values at pH6.0 (filled circles or squares) or pH7.4 (open circles or squares) were determined by GraphPad Prism software. Red color for the non-CAB antibody and blue color for BA302. x-axis: log antibody concentration in ng/mL; y-axis: Optical Density at 450 nm (OD450nm).

diluted in pH flow cytometry assay buffer were added to the cells and incubated for 1 h at 4°C in the dark with shaking. The mixture containing cells and antibodies was spun down and washed with the corresponding pH flow cytometry assay buffer three times. Secondary antibody (goat anti-human IgG, Invitrogen, catalog no. A11013) conjugated with fluorophore Alexa 488 was then added to each well and incubated for 45 min at 4°C in the dark with shaking. Cells were then washed with pH assay buffer three times and fixed with 4% paraformaldehyde (Polyscience Inc. catalog no. 18814-10). The median fluorescence intensity (MFI) was calculated using a NovoCyte flow cytometer (ACEA Biosciences, model 2060 R). MFI and antibody concentrations were used to generate 4-parameter nonlinear regression curves with variable slope using GraphPad Prism software version 7.03.

Kinetic analysis of pH-dependent binding of BA3021

Binding kinetics of BA3021 to human ROR2 were analyzed by surface plasmon resonance (SPR) on an SPR 2/4 instrument (Sierra Sensors, Hamburg, Germany). In brief, varying antibody concentrations were injected over a sensor surface with immobilized HuROR2. Binding kinetics were analyzed with the provided analysis software (Sierra Analyzer R2) with a 1:1 binding model. A molecular weight of 150 kDa was used to calculate the molar concentrations of the BA3021 analyte.

Receptor density

The ROR2 expression levels on 293-HuROR2 and 293-CynoROR2 cells were estimated using QuantiBrite™ phycoerythrin (PE) quantitation kit (BD, catalog no. 340495), which contains a mixture of beads that are loaded with known quantities of PE molecules (high, medium, and low). The logarithmic geometric mean of PE fluorescence intensity from the beads, and the number of PE molecules per bead provided by the vendor, was used to generate a standard curve. The ROR2 expressing cells were stained with an anti-ROR2 PE-conjugated antibody (R&D Systems, catalog no. FAB20641P), and the copy number of ROR2 receptors on the cells was calculated by extrapolation from the bead standard curve using the logarithmic geometric mean of PE fluorescence on stained cells (Figure S2).

In vitro cytotoxicity

The cytotoxicity of BA3021 or isotype control (B12-MMAE) was tested with ROR2 expressing cell lines. Cells were seeded in 50 µL of pH assay medium (DMEM +1×NEAA +1×sodium pyruvate + 10% FBS, adjusted to pH6.0 or pH7.4) at 3000 cells per well for human or cyno ROR2 expressing 293 stable clones (293-HuROR2 or 293-CynoROR2) or 2000 cells per well for LCLC103H or HT1080 in 96-well tissue culture-treated plates and incubated for 2–3 h in a humidified incubator containing 5% CO₂ at 37°C. Serial dilutions of 2X BA3021 stock solution at pH6.0 or pH7.4 assay media (50 µL per well) were added to the plates. After a 3-d incubation, the cell viability was measured with the CellTiter-Glo (Promega Corporation) reagent, and the luminescence was recorded on the SpectraMax i3X

plate reader. The inhibition rate (IR) of BA3021 or isotype antibody was determined by the following formula: IR (%) = (1-(RLU compound/RLU control)) × 100%. The inhibition rate of different doses was plotted in concentration-response inhibition curve, and half-maximal inhibitory concentration (IC₅₀) values were calculated. The data were interpreted using GraphPad Prism software using a four-parameter logistic nonlinear regression model.

In vivo efficacy study

Antitumor efficacy of BA3021 and the unconjugated parent antibody BA302 were assessed using different cell line-derived xenograft (CDX) models, including melanoma cancer cell line SK-MEL5 and lung cancer cell line LCLC-103 h (both studies were performed at Crown Bioscience, San Diego, California, USA).

Female NOD/SCID mice were implanted with 5×10^6 SK-MEL5 tumor cells or 20×10^6 LCLC-103 h tumor cells subcutaneously into the rear flank. When the tumor volume reached 100–150 mm³, the animals were randomized into groups of eight animals and treated intravenously (IV) with either vehicle, BA302, or BA3021 (once every 4 d, total of six injections). Tumor sizes were monitored routinely, and %TGI (tumor growth inhibition) was calculated (tumor volume change between the controls and test article-treated cohort).

For the *in vivo* efficacy study in patient-derived xenograft (PDX) models, low passage sarcoma models SA13179, SA10160, CTG-1079, CTG-0677, CTG-0714, GIST models GS11353, GS11327, GS11328, melanoma model CTG-0219, triple-negative breast cancer (TNBC) model CTG-1167, uterine cancer model CTG-1561, and colorectal model CTG-1951 were utilized (all studies were performed at Champion Oncology, Rockville, Maryland, US). Tumor fragments from the PDX models were implanted in female NOD-SCID mice. Tumor-bearing animals were randomized into treatment groups when the tumor volume reached approximately 150 mm³. Following randomization, the animals ($n = 3$ per group) were treated with vehicle (PBS) or BA3021 (6 mg/kg) once every 4 d for a total of four or six doses. Effects on tumor growth were evaluated by measuring percent TGI. Tolerability was assessed by body weight loss, lethality, and clinical signs of adverse treatment-related side effects. Body weights were measured twice a week.

In vivo toxicology and pharmacokinetics in non-human primates

The cynomolgus monkey was chosen as the only toxicology species due to the lack of cross-reactivity to the rodent ROR2 receptor. Nonclinical pharmacokinetics (PK) studies were conducted to evaluate the systemic exposure to BA3021, total antibody, and unconjugated MMAE in cynomolgus monkeys. The single- and repeat-dose PK of BA3021 was assessed in cynomolgus monkeys via IV administration. The plasma PK and serum anti-drug antibody (ADA) samples collected from a Good Laboratory Practice (GLP) toxicology study in cynomolgus monkeys were analyzed using validated bioanalytical methods (PPD Laboratories, USA). The PK data were analyzed

using the noncompartmental method and a semi-mechanistic modeling approach.

A non-GLP dose-range finding (DRF) study (SNBL USA, Ltd.) and a GLP compliant repeat-dose toxicity study were performed to evaluate the PK and toxicity of BA3021 in cynomolgus monkeys (WuXi AppTec Co., Ltd.). In the DRF study, male and female cynomolgus monkeys (one animal/sex/group) received BA3021 at 1, 3, and 10 mg/kg by IV bolus. Animals were observed for 21 d. Safety endpoints included clinical observations, food evaluation/consumption, body weight, hematology, coagulation, serum chemistry, and urinalysis. Blood was collected at multiple timepoints to characterize systemic exposure of BA3021, total antibody, and free-MMAE. At termination, gross observations and organ weights were recorded, and tissues were collected for microscopic evaluation.

In the repeat-dose toxicity study, BA3021 was administered by IV bolus in two doses, 3-week apart (Day 1 and Day 22) to male and female cynomolgus monkeys (5 animals/sex/group) at 0 (vehicle control), 1, 3, and 6 mg/kg/week. After the last dose, on Day 23 a necropsy was performed on surviving animals (5/sex/group), while the remaining animals were placed into a 4-week recovery period. Safety endpoints included clinical signs, body weights, ophthalmic exams, electrocardiogram (ECG), body temperature, clinical pathology (clinical chemistry, coagulation, hematology, and urinalysis), organ weights, as well as macroscopic and microscopic examinations. Blood samples were collected to evaluate systemic exposure to total ADC (BA3021), total antibody, free-MMAE, and for potential anti-drug antibodies (ADA). Exposure to total ADC and total antibody was assessed by immunoprecipitation, peptide digestion, and liquid chromatography/mass spectrometry (LC/MS analysis). Free-MMAE was measured by LC/MS. ADA was measured by MSD-electrochemiluminescence (ECL) method.

Results

Engineering of anti-ROR2 CABs

Novel antibodies against human ROR2 were developed targeting a ROR2-specific epitope close to the N-terminus to avoid cross reactivity with ROR1. ROR2-specific hybridomas were sequenced, expressed as chimeric IgG1 antibodies, and screened for cross reactivity with cynomolgus ROR2 and *in vitro* functional activities.

Chimeric clone BA-048-2-11 was selected for further engineering and the development of a conditionally active (CAB) antibody.^{37,38} The top humanized CAB lead, clone BA302, was conjugated with MMAE using a vedotin-type protease-cleavable linker, resulting in BA3021 (Figure 1a). The *in vitro* and *in vivo* characterization of the ADC, BA3021, is described below.

In vitro characterization of BA3021

The binding activity of BA3021 to human ROR2-ECD at pH6.0 (TME condition) and pH7.4 (physiological condition) was tested by pH affinity ELISA. BA3021 has strong binding to

human ROR2 at pH6.0 with an EC₅₀ of 56.3 ng/mL. At pH7.4, minimal binding was observed for the highest BA3021 concentration tested, but no meaningful EC₅₀ could be calculated (Figure 1b). BA3021 binding to human ROR2 was tested at pH5.5, 6.0, 6.2, 6.5, 6.7, 7.0, and 7.4 (pH range ELISA, Figure 1c). BA3021 had strong binding to human ROR2 at pH5.5 to ~pH6.4. At higher pH, the binding activity sharply dropped and only very little binding was detectable at pH7.0 - pH7.4. The pH inflection point (pH with 50% signal compared to pH6.0 set as 100%) was pH6.4. BA3021 binds to cynomolgus ROR2 at pH6.0 with a similar binding profile as to human ROR2 and had very little binding at pH7.4. (Figure 1d). BA3021 did not bind to mouse or rat ROR2 regardless of the pH (Figure 1d). In addition, BA3021 is highly specific for ROR2 and does not bind to human ROR1 (Figure 1e). The binding activity of naked BA3021 (BA302) to human ROR2-ECD at pH6.0 and pH7.4 conditions was tested by pH affinity ELISA along with non-CAB ROR2 antibody. BA302 shows a comparable strong binding as non-CAB antibody to human ROR2 at pH6.0 with an EC₅₀ of 11.9 ng/mL. The non-CAB antibody shows a similar EC₅₀ at pH7.4 as pH6.0, which is 9.7 ng/mL and 4.7 ng/mL, respectively. BA302 does not bind to human ROR2 well at pH7.4, and no meaningful EC₅₀ could be calculated (Figure 1f).

The binding activity of BA3021 to various ROR2-expressing cell lines at pH6.0 and pH7.4 was also measured by flow cytometry (Figure 2). BA3021 binds to cell-surface expressed ROR2 at pH 6.0, but very little binding was observed at pH7.4. BA3021 did not bind to naïve 293-F cells not expressing ROR2 on the surface (data not shown). There was no detectable binding of isotype control antibody (B12-MMAE) in any of the cell lines tested.

The binding kinetics of BA3021 at different pH values were determined by SPR. Representative sensorgrams for each pH condition are shown in Figure 3a. BA3021 showed a high affinity to human ROR2 at different pH values tested (Figure 3b). The affinity dropped from pH6.0 to pH7.4 about 5.7-fold, K_D [pH6.0] = 1.5 nM; K_D [pH7.4] = 8.6 nM. In addition to the lower affinity, the observed maximum SPR signal at pH7.4 reached only ~10% of the signal at pH6.0, which is characteristic of CABs.

In vitro cytotoxicity

The cytotoxicity of BA3021 to ROR2-expressing cell lines was initially assessed with HEK293 cells expressing human ROR2 (HuROR2) or cynomolgous ROR2 (CynoROR2) on the cell surface, both of which were engineered to highly express ROR2 (~220,000 copies of human and ~80,000 copies of cyno ROR2 based on PE staining). As shown in Figure 4a, b, BA3021 induced dose-dependent cytotoxicity in both stable cell lines. At pH6.0, IC₅₀ values were 280 ng/mL and 167 ng/mL for 293-HuROR2 and 293-CynoROR2, respectively. Lower levels of cytotoxicity were observed at pH7.4 for both cell lines. IC₅₀ data are summarized in Figure 4f. Cytotoxicity of the isotype ADC was observed only at the highest concentration tested. BA3021 also showed activity against LCLC103H and HT1080 cancer cell lines (Figures. 4c, d). Both cell lines express low levels of

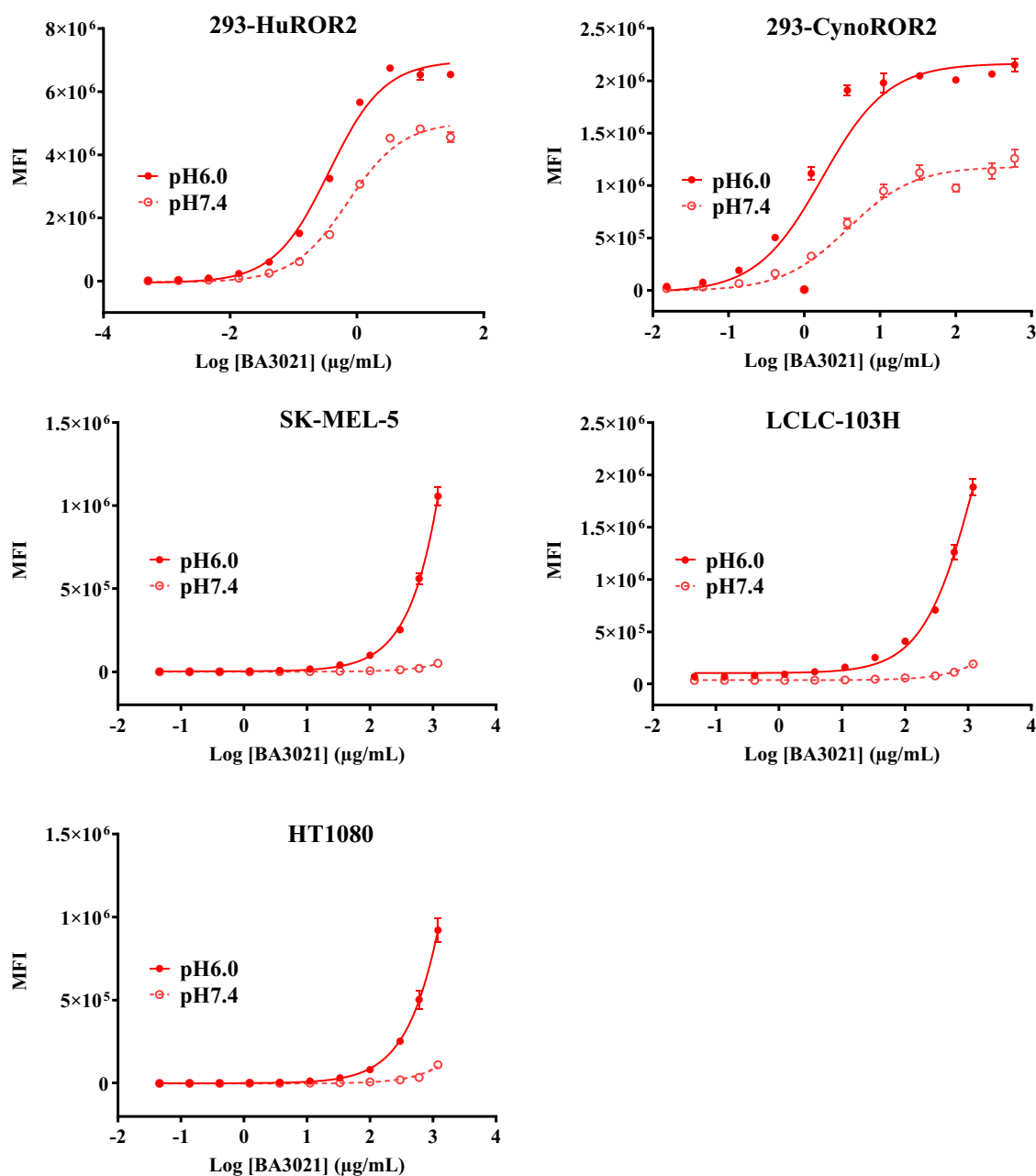


Figure 2. FACS analysis. Flow cytometric detection for antibody-specific binding to 293-HuROR2, 293-CynoROR2, SK-MEL-5, LCLC-103H, and HT1080 cells. Representative graphs. pH6.0: solid line; pH7.4: dashed line. x-axis: log BA3021 concentration in µg/mL; y-axis: Median Fluorescence Intensity (MFI).

ROR2 (the exact copy numbers could not be determined, as the signal with the commercial anti-ROR2-PE antibody was consistently low). BA3021 did not have a cytotoxic effect on ROR2-negative cells (Figure 4e). These findings collectively demonstrate that BA3021 mediates cytotoxicity in a concentration-dependent manner and achieves more potent cell-killing activity under tumor microenvironment conditions.

BA3021 inhibits tumor growth *in vivo*

The *in vivo* activity of BA3021 was evaluated in several CDX and PDX models representing different cancer indications.

BA3021 exhibited potent antitumor activity in an SK-MEL5 melanoma CDX model at doses of 6 and 10 mg/kg, with tumor

growth inhibition of 106% and 116%, respectively, at Day 33 (Figure 5a).

The efficacy of BA3021 was also evaluated in the LCLC103H human lung cancer xenograft model, in which BA3021 also showed strong dose-dependent antitumor activity. Treatment with BA3021 at 1 mg/kg moderately inhibited tumor growth, while treatment with BA3021 at 3 and 6 mg/kg resulted in complete tumor regression (Figure 5b). There was no observed tumor regression in the groups with unconjugated parental antibody BA302, in which the animals were administered with the same highest doses as the ones in BA3021-treated groups. Collectively, results from these *in vivo* xenograft studies demonstrate that BA3021 treatment can lead to effective anti-tumor responses.

Anti-tumor activity of BA3021 was evaluated in several PDX models. Treatment with BA3021 at 6 mg/kg

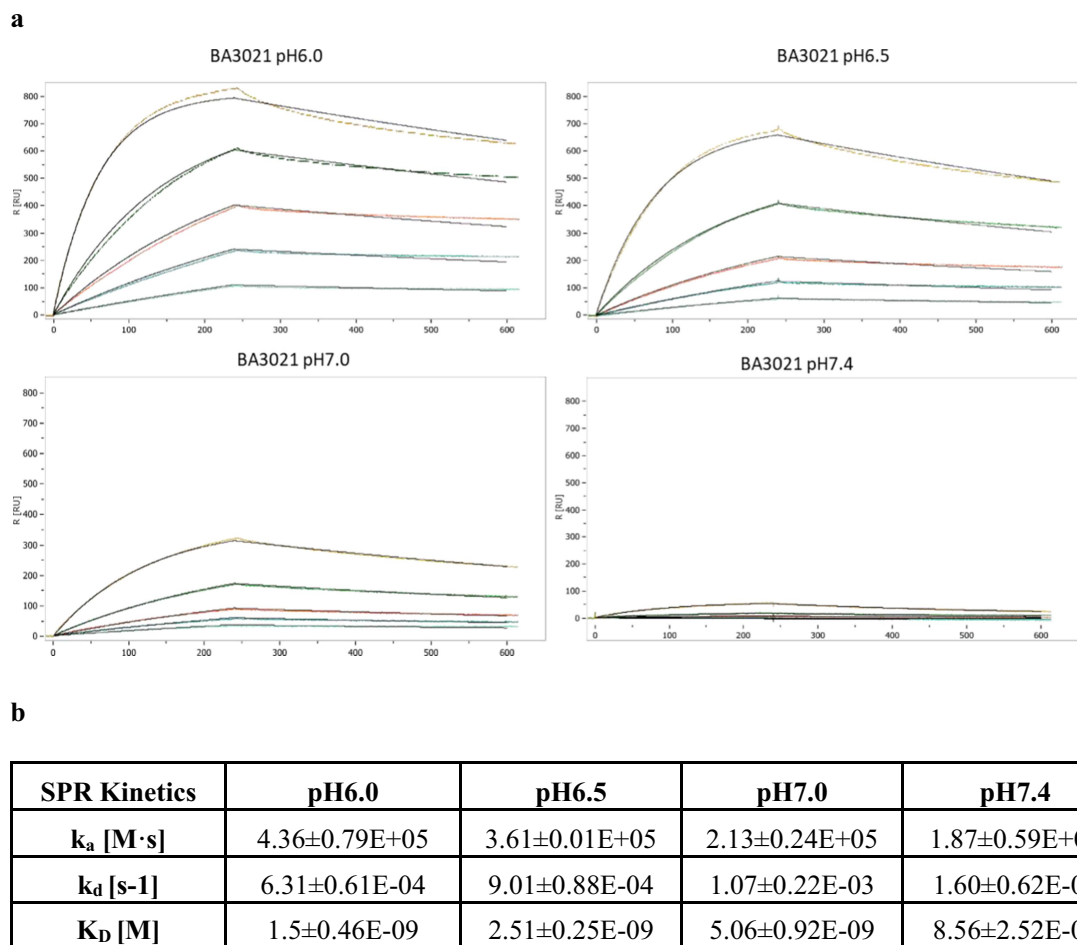


Figure 3. BA3021 binding kinetics measured by SPR. Kinetic analysis of BA3021 binding to human ROR2 at pH6.0, pH6.5, pH7.0, and pH7.4. Kinetic analysis was performed on an SPR2/4 instrument (Sierra Sensors) using a multicycle protocol injecting five different concentrations of BA3021 and buffer only. Three independent experiments were conducted at each pH. A: Representative sensorgrams for pH6.0 (top left), pH6.5 (top right), pH 7.0 (bottom left), and pH7.4 (bottom right). The same chip was used for all runs. The maximum signal drops from ~800 RU at pH6.0 to ~700 RU at pH6.5, and to ~300 RU at pH7.0, ~50 RU at pH7.4 based on the pH sensitive binding of BA3021. x-axis: time [s]; y-axis: Response units [RU]. B: Calculated binding kinetics of BA3021 to human ROR2. The binding affinity drops from 1.5 nM at pH6.0 to 2.5 nM at pH6.5, and to 5.1 nM at pH7.0, 8.6 nM at pH7.4. In addition, the maximum SPR signal drops ~16-fold from pH6.0 to pH7.4.

eradicated sarcoma SA13179 tumors (Figure 5c) and completely inhibited the growth of the gastrointestinal tumor, GS11353 (Figure 5d). Treatment with BA3021 at 6 mg/kg induced greater than 40% TGI in other PDX models (Table S1), suggesting that BA3021 has activity in a wide range of tumor types including sarcoma, GIST, melanoma, TNBC, uterine cancer, and colorectal cancer.

Pharmacokinetic, safety, and tolerability analysis of BA3021 in non-human primates

The PK profile of BA3021 in cynomolgus monkeys was determined after a single IV dose of 1, 3, or 10 mg/kg. Plasma concentration of unconjugated MMAE (Free MMAE) peaked at 1–2 d post dose (Figure 6a). The maximum concentration (C_{max}), area under the curve extrapolated to infinity (AUC_{inf}), and half-life ($t_{1/2}$) from the noncompartmental analysis of the PK data are presented in Figure 6b. The AUC of each analyte showed a slightly greater than dose proportional increase, suggesting the presence of a saturable elimination process for BA3021.⁴³

In the definitive GLP repeat-dose toxicity study of BA3021, there were no detectable ADC, total Ab, or unconjugated MMAE in samples analyzed from control groups. In general, the peak plasma BA3021 (Total ADC) concentration (C_{max}) was dose-proportional (Figure 6c, d). The peak plasma levels of unconjugated MMAE occurred 24 h post-dose (Figure 6c). Mean $AUC_{0-\tau}$, where τ is the dosing interval of 3 weeks (504 h), increased from 580 to 1,870 to 4,450 $\mu\text{g}\cdot\text{h}/\text{mL}$ over the dose range of 1, 3, and 6 mg/kg for the first dose given on Day 1. Similar AUC_{τ} was observed for the last dose (Day 22) with mean values of 637, 2,130, and 4,310 $\mu\text{g}\cdot\text{h}/\text{mL}$ for the three different dose levels, respectively. Mean clearance (CL) ranged from 1.36 to 1.75 mL/kg/h for Day 1 and from 1.45 to 1.59 mL/kg/h for Day 22, suggesting no change in TK and no accumulation. Mean plasma $t_{1/2}$ determined on Days 1 and 22 ranged from 39 to 71 h (Figure 6d).

Anti-BA3021 antibodies were detected in some of the plasma samples collected on Day 22 within each BA3021 treatment group and represented 30% of low dose (1 mg/kg/dose) animals (3 of 10 animals), 30% of mid dose (3 mg/kg/dose) animals (3 of 10 animals), and 10% of high dose (6 mg/kg/dose) animals (3 of 10 animals).

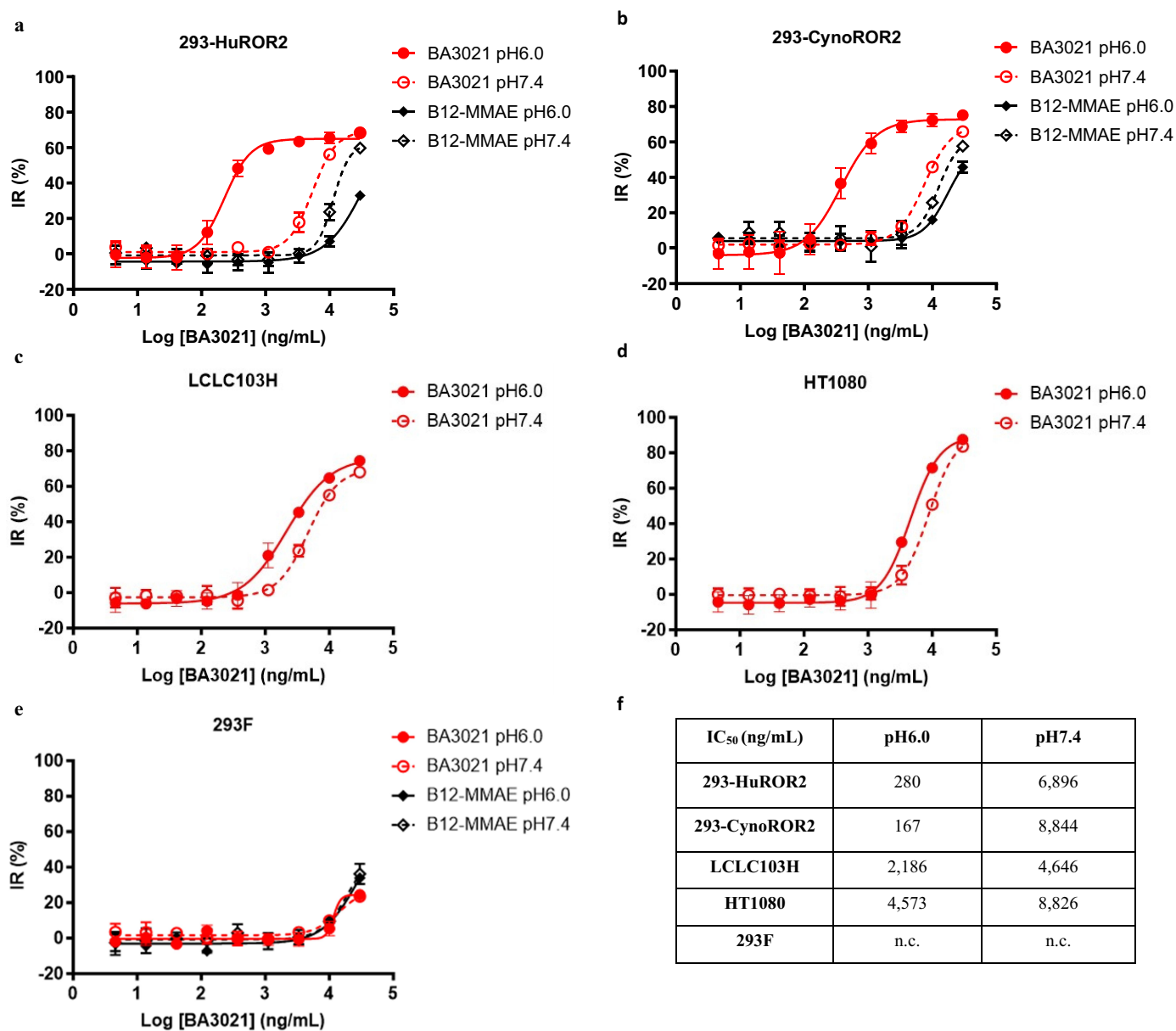


Figure 4. *In vitro* cytotoxicity of BA3021 at pH6.0 and pH7.4. Viability of cell line 293-HuROR2 cells (A) or 293-CynoROR2 cells (B) or LCLC103H (C) or HT1080 (D) or 293F (E) after a 3-d incubation period with the indicated ADCs was analyzed with a Cell Titer Glo viability assay. Inhibition rate (IR) was calculated as described in Materials and Methods. (F) Summary of Half-Maximal Inhibitory Concentration (IC₅₀) values in ng/mL. Each data point represents the mean of duplicate wells. x-axis: log ADC concentration in ng/mL; y-axis: Inhibition rate; N.A., not applicable

kg/dose) animals (1 of 10 animals). No apparent change in the PK characteristics of BA3021 or its components (total antibody and unconjugated MMAE) was associated with the presence of anti-BA3021 antibodies.

In a single-dose exploratory toxicity study in cynomolgus monkeys, bolus IV administration of BA3021 was well tolerated at the highest dose tested (10 mg/kg). There were no unscheduled deaths or morbidity in this study. Test article-related changes were confined to decreased white blood cell counts, particularly neutrophils. There was a dose-dependent decrease in neutrophil counts 7 d after dosing, which rebounded by Day 21. Also, BA3021-induced (10 mg/kg dose) decreases in CD3⁺, CD3⁺CD4⁺, CD3⁺CD8⁺, CD3⁻CD20⁺, or CD3⁻CD14⁺ cells were transient, as all cell types recovered on or before Day 21. Among these decreased

cells, there was also a notable change in cell counts of the monocyte population (CD3⁻CD14⁺) with an effect at 3 and 10 mg/kg. The effect of BA3021 on this population was reversible and monocyte counts rebounded to values exceeding pretest levels on Day 14. The exposure between males and females was similar and dose-proportional based on C_{max} values and AUC_{inf}. Based on the tolerability data for BA3021 in this study, the maximum tolerated dose (MTD) was 10 mg/kg. At 10 mg/kg, the mean BA3021 exposure (AUC_{inf}⁵) was 8,210 µg·h/mL and the C_{max} was 208 µg/mL, while the t_{1/2} was 116 h (Figure 6b). The AUC_{inf} and C_{max} levels of the released MMAE payload were 6.8 × 10⁻² µg·h/mL and 6.2 × 10⁻⁴ µg/mL, respectively (Figure 6b). The nonclinical safety profile of BA3021 has been also characterized with repeat-dose studies up to one-month in duration, including the assessment

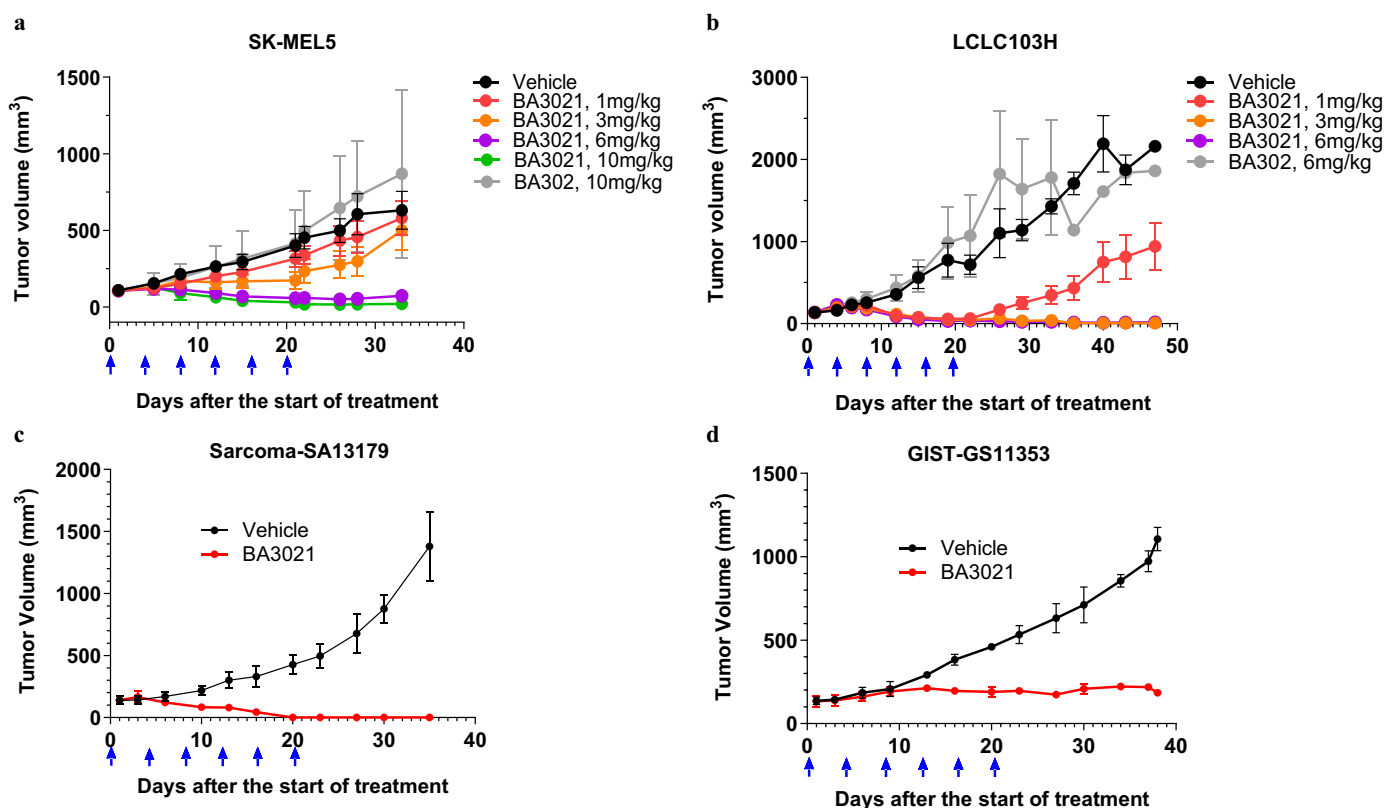


Figure 5. *In vivo* efficacy of BA3021 in CDX and PDX models. Cytotoxicity of BA3021 was tested in several cell-line derived xenograft models (CDX) and patient-derived xenograft models (PDX) in mice. In each model above, tumor growth was monitored routinely. The dosing dates were marked as blue arrows in the figures. x-axis: days after the start of treatment; y-axis: tumor volume in mm³. a and b: In CDX model, female NOD/SCID mice were implanted with SK-MEL5 tumor cells (A) or LCLC103H tumor cells (B) subcutaneously into the rear flank. When tumor volume reached 100–150 mm³, animals were randomized into groups of eight animals and treated intravenously with either vehicle, BA3021, or BA302 (Q4Dx6, once every 4 d, a total of six injections). c and d: BA3021 suppressed the tumor growth in Sarcoma SA13179 (C) and GIST GS11353 (D) models. The tumor fragments from the PDX models were implanted in female NOD-SCID mice. Tumor-bearing animals were randomized into treatment groups when the tumor volume reached approximately 150 mm³. Following randomization, animals ($n = 3$ per group) were treated with vehicle (PBS), or BA3021 (6 mg/kg) once every 4 d (Q4D) for six doses. Tumor growth curves of the indicated models are shown as mean tumor volumes. Error bars represent standard error of the mean (SEM).

of reversibility of toxicological effects. In both single- and repeat-dose studies, decreases in white blood cell parameters occurred in a dose-dependent manner. The effect on the hematopoietic system was completely reversible, as there were no remarkable findings after the one-month recovery period.

Discussion

ROR2 is expressed in many different cancer types and is often associated with more aggressive tumors and poor prognosis. Therapeutic strategies targeting ROR2 present a promising new approach for cancer treatment, but few such molecules are currently in development. In this report, we describe the preclinical development and characterization of BA3021, a first-in-class CAB ADC specific for ROR2. First, we generated novel ROR2-specific antibodies from hybridomas, humanized the lead antibody, and screened a library of variants for conditional binding to ROR2 in the TME. CAB generation was performed as previously described.³⁷ BA3021 was characterized by *in vitro* binding ELISA and cytotoxicity assays that mimic the acidic pH conditions of the TME. BA3021 demonstrated tumor-selective binding to human and cynomolgus ROR2,

with a pH inflection point at pH6.4 (*i.e.*, 50% binding signal compared to pH6.0) and minimal binding at normal physiological alkaline pH (\geq pH7.4) in an affinity ELISA assay. When the binding kinetics of BA3021 were analyzed by SPR, we observed a simultaneous decrease in both affinity and maximum signal with pH changes from pH6.0 to pH7.4. We have previously shown that this signal drop is caused by a change in the reversible availability of the reactive ligands on the sensor surface. The number of available reactive ligands drops with an increase in pH. The availability of reactive ligands at different pH conditions is affected by the interaction of the proteins with PaCS molecules, *i.e.*, bicarbonate ions, which block the binding of BA3021 in a concentration-dependent manner. Therefore, the pH selectivity is a combination of the change in K_D and the fold change in the maximum signal observed.^{37,38} Flow cytometry analysis showed that BA3021 demonstrated strong binding to various human cancer cell lines at acidic pH, but very little binding under normal physiologic alkaline conditions.

BA3021 demonstrated *in vitro* anti-cancer activity in a pH-dependent manner. Cell-growth inhibition by BA3021 was observed in melanoma and NSCLC cell lines at lower pH conditions. BA3021 was also tested in CDX mouse models and exhibited dose-dependent antitumor activity *in vivo*.

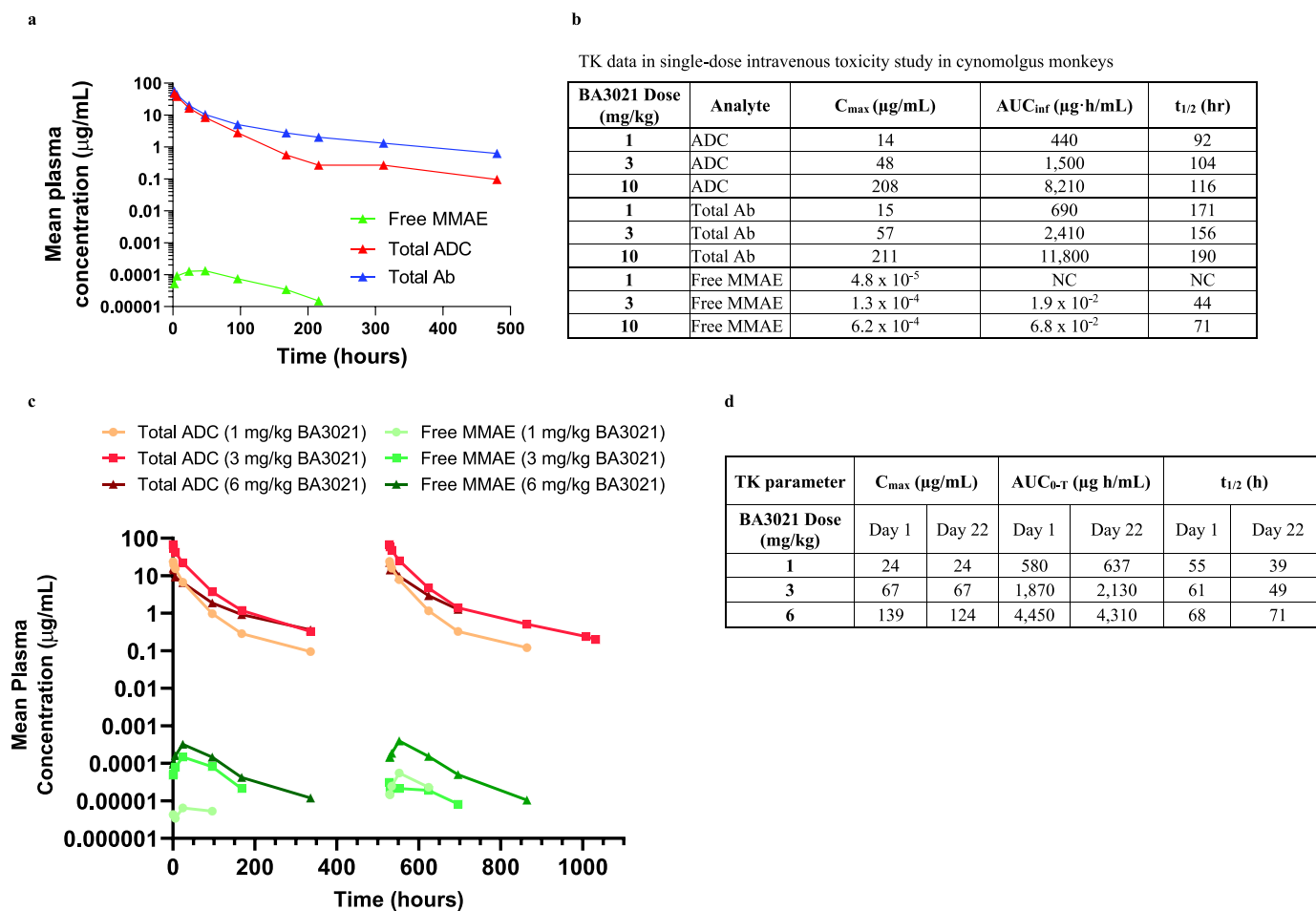


Figure 6. Pharmacokinetic and toxicokinetic analysis of BA3021 in non-human primates. **a:** PK Analysis for a single dose non-GLP study of BA3021 in cynomolgus monkeys. Mean plasma concentrations of total ADC, total Ab and free MMAE from cynomolgus monkeys (one female and one male) were determined after a single intravenous dose of 3 mg/kg. Plasma samples were collected post-dose at 2, 6, 24, 48, 96, 168, 216, 312, 480 h. x-axis: time after injection in hours; y-axis: mean plasma concentrations in µg/mL. **b:** Summary of TK parameters for BA3021, total Ab and free-MMAE in cynomolgus monkeys. The C_{max}, AUC_{inf} and t_{1/2} in cynomolgus monkeys (1 monkey/sex/dose) were determined after a single intravenous dose of 1, 3, and 10 mg/kg. NC, not calculated. **c:** PK Analysis for repeat doses of BA3021 in cynomolgus monkeys. The cynomolgus monkeys (10 monkey/sex/dose) were given BA3021 via intravenous injection at 1, 3 or 6 mg/kg for a total of 2 doses on Days 1 and 22. Plasma samples were collected post-dose at 0.5, 2, 6, 24, 96, 168, 336, 528 h. Mean plasma concentration of total ADC (BA3021) and free MMAE from cynomolgus monkeys was determined after the first dose on Day 1 and second dose on Day 22. x-axis: time after the first injection in hours; y-axis: mean plasma concentrations in µg/mL. **d:** TK data of BA3021 in repeat-dose intravenous toxicity study in cynomolgus monkeys. The cynomolgus monkeys were given BA3021 via intravenous injection at 1, 3 or 6 mg/kg for a total of 2 doses on Days 1 and 22.

BA3021 significantly inhibited the tumor growth of NSCLC and melanoma cancer xenografts. In all the studies described herein, the parental unconjugated antibody BA302 was included as a control for efficacy and showed no antitumor activity in these tumor models. We do not know if the CAB-selective binding influences the efficacy of BA3021 compared to the non-CAB parental clone, as it was not included in the efficacy studies. However, we performed a detailed efficacy study for our EpCAM-targeting T cell engager and showed that the pH-selective binding has no impact on its efficacy in a mouse model.³⁸

The nonclinical safety profile of BA3021 has been characterized through single- and repeat-dose studies lasting up to one-month, including an assessment of the reversibility of toxicological effects. BA3021 was well tolerated following single or repeat IV dosing. Neither morbidity nor mortality was observed in the monkeys. Test article-related hematological changes were not associated with adverse pathological changes in lymphoid organs, and all findings were reversible following

a 4-week recovery period. In the repeat-dose study, a few animals tested positive for anti-BA3021 antibodies; however, despite the ADA response, there was no effect on BA3021 exposure, and no ADA-associated toxicities were observed. The nonclinical safety findings with BA3021 were consistent with toxicities observed with other MMAE-containing ADCs and are easily monitored, reversible, and present a controllable and acceptable risk in the targeted patient group. The non-clinical safety profile of BA3021 supports clinical development in advanced cancer indications. BA3021 (ozuriftamab vedotin) is currently in multiple Phase 2 clinical trials with several solid tissue tumor settings. Multiple objective responses have been observed with ozuriftamab vedotin among patients with heavily pretreated HPV-positive oropharyngeal cancer, with acceptable tolerability,⁴⁴ including one complete response [Eric Sievers, personal communication⁴⁴]. Future clinical trials are planned to further investigate the promising antitumor activity in patients with HPV-driven cancers associated with ROR2 overexpression.

Acknowledgments

We thank BioDuro-Sundia Discovery Biology Team for their valuable technical assistance and R&D support; Monica Sullivan and James Butler for critical reading of the manuscript; and Dr Leslie L. Sharp for helping with the design and support of the *in vivo* murine models and non-human primate studies.

We also thank Eilidh Williamson for medical writing assistance.

Disclosure statement

All authors are shareholders of BioAtla, Inc., which owns intellectual property rights to CABs- and PaCS-related technology. HWC, GF, and JMS are inventors of relevant patents. JMS serves as a Director of BioAtla.

Funding

The author(s) reported that there is no funding associated with the work featured in this article.

ORCID

Hwai Wen Chang  <http://orcid.org/0000-0001-8666-2002>
 Gerhard Frey  <http://orcid.org/0000-0003-2086-4853>
 Jing Wang  <http://orcid.org/0009-0005-7067-9316>
 Haizhen Liu  <http://orcid.org/0000-0002-6268-5485>
 Charles Xing  <http://orcid.org/0000-0002-5108-3577>
 Jian Chen  <http://orcid.org/0000-0001-8105-3670>
 William J. Boyle  <http://orcid.org/0000-0001-5304-5649>
 Jay M. Short  <http://orcid.org/0000-0001-7661-6854>

References

- Endo M, Kamizaki K, Minami Y. The Ror-family receptors in development, tissue regeneration and age-related disease. *Front Cell Dev Biol.* 2022;10:891763. doi: 10.3389/fcell.2022.891763.
- Stricker S, Rauschenberger V, Schambony A. ROR-Family receptor Tyrosine Kinases. *Curr Top Dev Biol.* 2017;123:105–142. doi: 10.1016/bs.ctdb.2016.09.003.
- Green JL, Kuntz SG, Sternberg PW. Ror receptor tyrosine kinases: orphans no more. *Trends Cell Biol.* 2008;18(11):536–544. doi: 10.1016/j.tcb.2008.08.006.
- Henry C, Quadir A, Hawkins NJ, Jary E, Llamas E, Kumar D, Daniels, B., Ward, R.L., Ford, C.E. Expression of the novel wnt receptor ROR2 is increased in breast cancer and may regulate both beta-catenin dependent and independent wnt signalling. *J Cancer Res Clin Oncol.* 2015;141(2):243–254. doi: 10.1007/s00432-014-1824-y.
- Oishi I, Suzuki H, Onishi N, Takada R, Kani S, Ohkawara B, Koshida I, Suzuki K, Yamada G, Schwabe GC, et al. The receptor tyrosine kinase Ror2 is involved in non-canonical Wnt5a/jnk signalling pathway. *Genes Cells.* 2003;8(7):645–654. doi: 10.1046/j.1365-2443.2003.00662.x.
- Rasmussen NR, Wright TM, Brooks SA, Hacker KE, Debebe Z, Sendor AB, Walker MP, Major MB, Green J, Wahl GM, et al. Receptor tyrosine kinase-like orphan receptor 2 (Ror2) expression creates a poised state of wnt signaling in renal cancer. *J Biol Chem.* 2013;288(36):26301–26310. doi: 10.1074/jbc.M113.466086.
- Yamamoto H, Yoo SK, Nishita M, Kikuchi A, Minami Y. Wnt5a modulates glycogen synthase kinase 3 to induce phosphorylation of receptor tyrosine kinase Ror2. *Genes Cells.* 2007;12(11):1215–1223. doi: 10.1111/j.1365-2443.2007.01128.x.
- Matsuda T, Nomi M, Ikeya M, Kani S, Oishi I, Terashima T, Takada S, Minami Y. Expression of the receptor tyrosine kinase genes, Ror1 and Ror2, during mouse development. *Mechanisms Of Devel.* 2001;105(1–2):153–156. doi: 10.1016/S0925-4773(01)00383-5.
- Nomi M, Oishi I, Kani S, Suzuki H, Matsuda T, Yoda A, Kitamura M, Itoh K, Takeuchi S, Takeda K, et al. Loss of mRor1 enhances the heart and skeletal abnormalities in mRor2-deficient mice: redundant and pleiotropic functions of mRor1 and mRor2 receptor tyrosine kinases. *Mol Cell Biol.* 2001;21(24):8329–8335. doi: 10.1128/MCB.21.24.8329-8335.2001.
- Takeuchi S, Takeda K, Oishi I, Nomi M, Ikeya M, Itoh K, Tamura S, Ueda T, Hatta T, Otani H, et al. Mouse Ror2 receptor tyrosine kinase is required for the heart development and limb formation. *Genes Cells.* 2000;5(1):71–78. doi: 10.1046/j.1365-2443.2000.00300.x.
- Afzal AR, Rajab A, Fenske CD, Oldridge M, Elanko N, Ternes-Pereira E, Tüysüz B, Murday VA, Patton MA, Wilkie AOM, et al. Recessive robinow syndrome, allelic to dominant brachydactyly type B, is caused by mutation of ROR2. *Nat Genet.* 2000;25(4):419–422. doi: 10.1038/78107.
- Schwabe GC, Tinschert S, Buschow C, Meinecke P, Wolff G, Gillissen-Kaesbach G, Oldridge M, Wilkie AOM, Kömec R, Mundlos S. Distinct mutations in the receptor tyrosine kinase gene ROR2 cause brachydactyly type B. *Am J Hum Genet.* 2000;67(4):822–831. doi: 10.1086/303084.
- Carrero I, Liu HC, Sikora AG, Milosavljevic A. Histoepigenetic analysis of HPV- and tobacco-associated head and neck cancer identifies both subtype-specific and common therapeutic targets despite divergent microenvironments. *Oncogene.* 2019;38(19):3551–3568. doi: 10.1038/s41388-018-0659-4.
- Avincsal MO, Kamizaki K, Jimbo N, Shinomiya H, Nibu KI, Nishita M, Minami Y. Oncogenic E6 and/or E7 proteins drive proliferation and invasion of human papilloma virus-positive head and neck squamous cell cancer through upregulation of Ror2 expression. *Oncol Rep.* 2021;46(1). doi: 10.3892/or.2021.8099.
- Yoda A, Oishi I, Minami Y. Expression and function of the Ror-family receptor tyrosine kinases during development: lessons from genetic analyses of nematodes, mice, and humans. *J Recept Signal Transduct Res.* 2003;23(1):1–15. doi: 10.1081/rrs-120018757.
- John M, Ford CE. Pan-tissue and -cancer analysis of ROR1 and ROR2 transcript variants identify novel functional significance for an alternative splice variant of ROR1. *Biomedicines.* 2022;10(10):2559. doi: 10.3390/biomedicines10102559.
- Masiakowski P, Carroll RD. A novel family of cell surface receptors with tyrosine kinase-like domain. *J Biol Chem.* 1992;267(36):26181–26190. doi: 10.1016/s0021-9258(18)35733-8.
- Rozen EJ, Shohet JM. Systematic review of the receptor tyrosine kinase superfamily in neuroblastoma pathophysiology. *Cancer Metastasis Rev.* 2022;41(1):33–52. doi: 10.1007/s10555-021-10001-7.
- Morioka K, Tanikawa C, Ochi K, Daigo Y, Katagiri T, Kawano H, Kawaguchi, H., Myoui, A., Yoshikawa, H., Naka, N., et al. Orphan receptor tyrosine kinase ROR2 as a potential therapeutic target for osteosarcoma. *Cancer Sci.* 2009;100(7):1227–1233. doi: 10.1111/j.1349-7006.2009.01165.x.
- Rasmussen NR, Debebe Z, Wright TM, Brooks SA, Sendor AB, Brannon AR, Hakimi AA, Hsieh JJ, Choueiri TK, Tamboli P, et al. Expression of Ror2 mediates invasive phenotypes in renal cell carcinoma. *PLoS One.* 2014;9(12):e116101. doi: 10.1371/journal.pone.0116101.
- Wright TM, Rathmell WK. Identification of Ror2 as a hypoxia-inducible factor target in von Hippel-Lindau-associated renal cell carcinoma. *J Biol Chem.* 2010;285(17):12916–12924. doi: 10.1074/jbc.M109.073924.
- Yang CM, Ji S, Li Y, Fu LY, Jiang T, Meng FD. Ror2, a developmentally regulated kinase, is associated with tumor growth, apoptosis, migration, and invasion in renal cell carcinoma. *Oncol Res.* 2017;25(2):195–205. doi: 10.3727/096504016X14732772150424.
- O'Connell MP, Marchbank K, Webster MR, Valiga AA, Kaur A, Vultur A, Li L, Herlyn M, Villanueva J, Liu Q, et al. Hypoxia induces phenotypic plasticity and therapy resistance in melanoma

- via the tyrosine kinase receptors ROR1 and ROR2. *Cancer Discov.* 2013;3(12):1378–1393. doi: [10.1158/2159-8290.CD-13-0005](https://doi.org/10.1158/2159-8290.CD-13-0005).
24. Mei H, Lian S, Zhang S, Wang W, Mao Q, Wang H. High expression of ROR2 in cancer cell correlates with unfavorable prognosis in colorectal cancer. *Biochem Biophys Res Commun.* 2014;453(4):703–709. doi: [10.1016/j.bbrc.2014.09.141](https://doi.org/10.1016/j.bbrc.2014.09.141).
 25. Huang J, Fan X, Wang X, Lu Y, Zhu H, Wang W, Zhang S, Wang Z. High ROR2 expression in tumor cells and stroma is correlated with poor prognosis in pancreatic ductal adenocarcinoma. *Sci Rep.* 2015;5(1):12991. doi: [10.1038/srep12991](https://doi.org/10.1038/srep12991).
 26. Lu C, Wang X, Zhu H, Feng J, Ni S, Huang J. Over-expression of ROR2 and Wnt5a cooperatively correlates with unfavorable prognosis in patients with non-small cell lung cancer. *Oncotarget.* 2015;6(28):24912–24921. doi: [10.18632/oncotarget.4701](https://doi.org/10.18632/oncotarget.4701).
 27. Zhang W, Yan Y, Gu M, Wang X, Zhu H, Zhang S, Wang, W. High expression levels of Wnt5a and Ror2 in laryngeal squamous cell carcinoma are associated with poor prognosis. *Oncol Lett.* 2017;14(2):2232–2238. doi: [10.3892/ol.2017.6386](https://doi.org/10.3892/ol.2017.6386).
 28. Edris B, Espinosa I, Muhlenberg T, Mikels A, Lee CH, Steigen SE, Zhu S, Montgomery KD, Lazar AJ, Lev D, et al. ROR2 is a novel prognostic biomarker and a potential therapeutic target in leiomyosarcoma and gastrointestinal stromal tumour. *J Pathol.* 2012;227(2):223–233. doi: [10.1002/path.3986](https://doi.org/10.1002/path.3986).
 29. Bayerlova M, Menck K, Klemm F, Wolff A, Pukrop T, Binder C, Beißbarth T, Bleckmann A. Ror2 signaling and its relevance in breast cancer progression. *Front Oncol.* 2017;7:135. doi: [10.3389/fonc.2017.00135](https://doi.org/10.3389/fonc.2017.00135).
 30. Roarty K, Pfefferle AD, Creighton CJ, Perou CM, Rosen JM. Ror2-mediated alternative wnt signaling regulates cell fate and adhesion during mammary tumor progression. *Oncogene.* 2017;36(43):5958–5968. doi: [10.1038/onc.2017.206](https://doi.org/10.1038/onc.2017.206).
 31. Da Forno PD, Pringle JH, Hutchinson P, Osborn J, Huang Q, Potter L, Hancox RA, Fletcher A, Saldanha GS. WNT5A expression increases during melanoma progression and correlates with outcome. *Clin Cancer Res.* 2008;14(18):5825–5832. doi: [10.1158/1078-0432.CCR-07-5104](https://doi.org/10.1158/1078-0432.CCR-07-5104).
 32. Menck K, Heinrichs S, Baden C, Bleckmann A. The WNT/ROR pathway in cancer: from signaling to Therapeutic intervention. *Cells.* 2021;10(1):142. doi: [10.3390/cells10010142](https://doi.org/10.3390/cells10010142).
 33. O'Connell MP, Fiori JL, Xu M, Carter AD, Frank BP, Camilli TC, French AD, Dissanayake SK, Indig FE, Bernier M, et al. The orphan tyrosine kinase receptor, ROR2, mediates Wnt5A signaling in metastatic melanoma. *Oncogene.* 2010;29(1):34–44. doi: [10.1038/onc.2009.305](https://doi.org/10.1038/onc.2009.305).
 34. Debebe Z, Rathmell WK. Ror2 as a therapeutic target in cancer. *Pharmacology & Therapeutics.* 2015;150:143–148. doi: [10.1016/j.pharmthera.2015.01.010](https://doi.org/10.1016/j.pharmthera.2015.01.010).
 35. Khongorzul P, Ling CJ, Khan FU, Ihsan AU, Zhang J. Antibody-Drug Conjugates: A Comprehensive Review. *Mol Cancer Res.* 2020;18(1):3–19. doi: [10.1158/1541-7786.MCR-19-0582](https://doi.org/10.1158/1541-7786.MCR-19-0582).
 36. Chen LQ, Howison CM, Jeffery JJ, Robey IF, Kuo PH, Pagel MD. Evaluations of extracellular pH within in vivo tumors using acidoCEST MRI. *Magn Reson Med.* 2014;72(5):1408–1417. doi: [10.1002/mrm.25053](https://doi.org/10.1002/mrm.25053).
 37. Chang HW, Frey G, Liu H, Xing C, Steinman L, Boyle WJ, Short JM. Generating tumor-selective conditionally active biologic anti-CTLA4 antibodies via protein-associated chemical switches. *Proc Natl Acad Sci USA.* 2021;118(9). doi: [10.1073/pnas.2020606118](https://doi.org/10.1073/pnas.2020606118).
 38. Frey G, Cugnetti APG, Liu H, Xing C, Wheeler C, Chang HW, Boyle WJ, Short JM. A novel conditional active biologic anti-EpCAM x anti-CD3 bispecific antibody with synergistic tumor selectivity for cancer immunotherapy. *Mabs-austin.* 2024;16(1):2322562. doi: [10.1080/19420862.2024.2322562](https://doi.org/10.1080/19420862.2024.2322562).
 39. Feng Q, Bennett Z, Grichuk A, Pantoja R, Huang T, Faubert B, Huang G, Chen M, DeBerardinis RJ, Sumer BD, et al. Severely polarized extracellular acidity around tumour cells. *Nat Biomed Eng.* 2024;8(6):787–799. doi: [10.1038/s41551-024-01178-7](https://doi.org/10.1038/s41551-024-01178-7).
 40. Rohani N, Hao L, Alexis MS, Joughin BA, Krismer K, Moufarrej MN, Soltis AR, Lauffenburger DA, Yaffe MB, Burge CB, et al. Acidification of tumor at stromal boundaries drives transcriptome alterations associated with aggressive phenotypes. *Cancer Res.* 2019;79(8):1952–1966. doi: [10.1158/0008-5472.CAN-18-1604](https://doi.org/10.1158/0008-5472.CAN-18-1604).
 41. Ho AL, Adkins D, Lorch JH, Thomas JS, Grewal JS. A phase 2 open-label study of conditionally active biologic ozuriftamab vedotin (BA3021) in failed PD-1/L1 treatment of patients with recurrent or metastatic squamous cell carcinoma of the head and neck. *J Clin Oncol.* 2023;41(16_suppl):TPS6107–TPS. doi: [10.1200/JCO.2023.41.16_suppl.TPS6107](https://doi.org/10.1200/JCO.2023.41.16_suppl.TPS6107).
 42. Doronina SO, Toki BE, Torgov MY, Mendelsohn BA, Cerveny CG, Chace DF, DeBlanc RL, Gearing RP, Bovee TD, Siegall CB, et al. Development of potent monoclonal antibody auristatin conjugates for cancer therapy. *Nat Biotechnol.* 2003;21(7):778–784. doi: [10.1038/nbt832](https://doi.org/10.1038/nbt832).
 43. Sorzano COS, Moreno MAP, Vilas JL. An analytical solution for saturable absorption in pharmacokinetics models. *Pharm Res.* 2023;40(2):481–485. doi: [10.1007/s11095-022-03455-z](https://doi.org/10.1007/s11095-022-03455-z).
 44. Wong W, Adkins DR, Misleh JG, Lorch J, Grewal JS, Russell J, Cetnar J, Ho AL, Chen K, Aysola K, et al. Phase II trial of ozuriftamab vedotin (BA3021), a conditionally active biologic (CAB)-ROR2-ADC, in patients with recurrent or metastatic squamous cell carcinoma of the head and neck (R/M SCCHN). *Ann Oncol.* 2024;35:S613–S55. doi: [10.1016/j.annonc.2024.08.929](https://doi.org/10.1016/j.annonc.2024.08.929).